Nonlinear Rheology of Multiarm Star Chains

Hiroshi Watanabe,* Yumi Matsumiya, and Satoshi Ishida

Institute for Chemical Research, Kyoto University, Uji, Kyoto 611-0011, Japan

Toshikazu Takigawa

Department of Material Chemistry, Faculty of Engineering, Kyoto University, Kyoto Daigaku Katsura, Nishikyo-ku, Kyoto 606-8510, Japan

Takashi Yamamoto

Venture Business Laboratory, Yamagata University, Jyonan 4-3-16, Yonezawa, Yamagata 992-8510, Japan

Dimitris Vlassopoulos

FORTH, Institute of electronic Structure & Laser and University of Crete, Department of Materials Science & Technology, Heraklion 71110, Crete, Greece

Jacques Roovers

National Research Council, Institute for Environmental Chemistry, Ottawa, Ontario, Canada K1A 0R6

Received April 1, 2005; Revised Manuscript Received June 22, 2005

ABSTRACT: In the linear viscoelastic regime, multiarm star chains having more than 24 arms bound by a soft core exhibit fast relaxation due to motion of individual arms and slow relaxation related to motion of the soft cores (structural rearrangement in a liquidlike order). In this regard, the multiarm stars are qualitatively similar to randomly dispersed polystyrene−polyisoprene (PS−PI) and polybutadiene−polystyrene (PB−PS) copolymer micelles, the former having rigid (glassy) PS cores and the latter with soft (rubbery) PB cores. However, the multiarm star PB chains and the copolymer micelles were found to exhibit significant rheological differences in the nonlinear regime possibly because of the differences in their core−arm (core−corona) compatibility and core softness. In long time scales, the nonlinear damping of the relaxation modulus measured for the multiarm star PB was much weaker than that for the micelles and somewhat similar to the damping of a critical gel. In contrast, the damping in short time scales was moderately stronger for the multiarm stars. A corresponding difference was observed for the viscosity under fast flow. These differences may be attributed to a strain-induced elastic coupling of the multiarm star chains: The soft core of the multiarm star, *chemically identical to the arms*, may become scarcer on application of large deformation to suck in some segments of neighboring star arms so as to preserve the segment density therein. Then, the multiarm star chains are elastically coupled/connected through these cores to form a huge transient network under large deformation, thereby increasing and decreasing the relaxation intensities in long and short time scales, respectively. This mechanism, being absent for the PS−PI and PB−PS micelles because of lack of the core−corona compatibility (as well as the core rigidity for the PS−PI micelles), would have led to the observed weakening and enhancement of the damping for the slow and fast processes of the multiarm stars.

1. Introduction

Multiarm star chains having more than 24 arms behave as a soft material exhibiting both polymeric and colloidal features. This star has a soft/deformable core in which its arm segments are highly crowded. Vlassopoulos and co-workers[1−6] extensively investigated the linear viscoelastic behavior and equilibrium dynamics of such multiarm stars and found that these stars exhibit fast and slow relaxation processes. The fast process is similar to the terminal relaxation process of *usual* star chains (having fewer than 24 arms) and attributable to relaxation of individual star arms. In this regard, the soft core binding of the multiarms has a rather minor effect on the fast process in the linear regime.

However, this soft core plays an essential role in the slow relaxation process of the multiarm star chains. The density of the segments of a focused star chain, being close to the bulk density in the core, decreases significantly with increasing distance from the core. Thus, the neighboring star chains thermodynamically interact with the focused chain to compensate this decrease, thereby giving rise to an excluded-volume effect in a length scale comparable to the chain dimension.[4] As a result, the multiarm stars form a liquidlike order in the spatial distribution of their soft cores.[2−4] The slow relaxation of these stars is attributable to structural rearrangements within this liquidlike order (random exchange of the core positions).[2−5]

These dynamic features of the multiarm stars are qualitatively similar, in many aspects, to the features of several classes of soft materials having some sort of cores. For example, polystyrene−polybutadiene (PS−PB) and polystyrene−polyisoprene (PS−PI) diblock copolymers form spherical micelles with rigid PS cores and solvated diene corona in diene-selective solvents such as *n*-tetradecane, and PB−PS copolymers form the

* To whom all correspondences should be addressed. E-mail hiroshi@scl.kyoto-u.ac.jp.

10.1021/ma0506738 CCC: $30.25
Published on Web 07/21/2005

micelles with soft PB cores and solvated PS corona in PS-selective solvents such as dibutyl phthalate. At relatively high concentrations, these micelles are arranged on cubic lattices due to the osmotic interaction between the corona blocks to exhibit static elasticity against small strains.[7−11] The cubic lattice has an infinitely long relaxation time under small strains, and its elasticity corresponds to the initial elasticity of the slow process of the multiarm stars having a finite relaxation time. Furthermore, the micellar lattice systems exhibit the relaxation of individual corona blocks in short time scales,[8,9,11] as similar to the behavior of the multiarm stars.

An even more direct similarity is found for the copolymer micelles in polymeric selective solvents, i.e., low-M homopolymers chemically identical to the micellar corona. In these solvents, the osmotic interaction between the corona blocks is screened and the micelles are randomly dispersed.[8,12] This micellar dispersion fully relaxes through fast and slow relaxation processes being attributed to the relaxation of individual corona blocks and the Stokes−Einstein (SE) diffusion of the micelles.[8,12−19] These relaxation mechanisms are similar to those of the multiarm stars.

Furthermore, solid nanoparticles (such as silica particles) are randomly suspended in appropriate media to exhibit a slow relaxation process reflecting their Brownian motion.[20−23] This relaxation process is similar to that of the slow processes of the multiarm stars and copolymer micelles, although the Brownian suspensions contain no flexible chain and exhibit no polymeric relaxation in short time scales.

The above *qualitative* similarities between the multiarm stars and various kinds of soft materials suggest that the equilibrium dynamics of the soft materials containing some sort of cores and/or particles is governed by the common physics. At the same time, the softness of the core and the core−arm (core−corona) interaction should have some *quantitative* effects on the relaxation. For example, the relaxation time τ_f of the fast process of the multiarm stars having the soft and fairly small cores is quantitatively close to the terminal relaxation time τ_{star} of usual stars having fewer than 24 arms[6] while τ_f of the PI corona of the PS−PI micelles is considerably larger than τ_{star} because of the steric hindrance from the rigid and large PS cores.[8,9] It is of interest to further investigate the effect of the core softness and the core−arm interaction on the dynamics of the soft materials.

In relation to this core effect, we remember that the PS−PI and PB−PS micellar dispersions (having rigid PS and soft PB cores, respectively) exhibit characteristic nonlinear damping against large step strains:[8,18,19,24] The damping for the fast relaxation process of the micelles reflects the nonlinear behavior of the corona blocks and its magnitude is close to that for the homopolymer chains. On the other hand, the damping in long time scales is attributable to the nonlinearity in the strain dependence of the anisotropy of the spatial distribution of the micelles. For the micelles having either rigid or soft cores, the damping for the slow process is much stronger than that for the fast process and similar to the damping observed for the random suspensions of Brownian particles.[8,18,19,24] This damping behavior is expected to change with the core−arm (core−corona) interaction as well as the core softness.

Table 1. Characteristics of the Multiarm Star PB Samples[25]

code	$10^{-3}M$	$10^{-3}M_{arm}$	f [a]
PB 64−30	1338	23.9	56
PB 64−60	2890	47.5	61
PB 64−80	4200	71	59

[a] Number of arms per star chain.

With this expectation, we have examined the nonlinear rheological behavior of the multiarm star PB chains and compared the results with the behavior of the PS−PI and PB−PS micellar dispersions. It turned out that the damping for the slow process of the multiarm stars, reflecting the nonlinearity in the structural rearrangement in the liquidlike order of these stars, is much weaker than that for the slow process of the micelles (having either rigid or soft cores). Corresponding differences were noted also for the nonlinear relaxation moduli for the fast process (arm relaxation) as well as for the viscosity under steady flow. Details of these differences are presented/discussed in this paper.

2. Experimental Section

2.1. Materials. Multiarm star 1,4-polybutadiene (PB) samples, anionically synthesized with a chlorosilane-modified dendrimer scaffold (coupler) and fully characterized in the previous study,[25] were utilized. Their molecular characteristics are summarized in Table 1. The sample code number indicates the nominal functionality of the coupler ($f = 64$) hyphened with the arm molecular weight M_{arm} (in unit of 1000) targeted in the synthesis. (This code is slightly different from the previous code,[25] the latter including no hyphen.) The characterization (light scattering and viscometry)[25] gave the f and M_{arm} values a little smaller than the nominal/targeted values, as shown in Table 1.

The systems subjected to the rheological measurements were blends of the multiarm star PB samples in an oligomeric butadiene (B2; Nisseki Co.; $M \cong 2 \times 10^3$, $M_w/M_n \cong 2$). These blends were prepared by first dissolving prescribed masses of the star PB and the matrix B2 in benzene at a concentration ≅5 wt % and then allowing benzene to thoroughly evaporate. The star PB concentrations were 20 wt % for the PB 64−30 sample, 40 wt % for the PB 64−60 sample, and 20 and 40 wt % for the PB 64−80 sample. The arms of neighboring stars were barely entangled in the 20 wt % PB 64−30/B2 blend while they were considerably entangled in the other blends,[26] as noted from comparison of the reduced molecular weight $M_{arm}\phi_{arm}^{1.3}$ (ϕ_{arm} = arm volume fraction in the blend) and the entanglement spacing for bulk 1,4-PB,[27] $M_e^\circ = 2.0 \times 10^3$. The matrix B2 is too short to exhibit any entanglement effect.

2.2. Measurements. For the multiarm star PB/B2 blends, rheological measurements were conducted with a laboratory rheometer (ARES, Rheometrics) in a cone−plate geometry of the plate diameter = 2.5 cm and the gap angle between cone and plate = 0.1 rad.

Nonlinear stress relaxation experiments against step strains of magnitude γ (≤4) were made at temperatures T_r/°C = −10, 20, 10, and 60 for the 20 wt % PB 64−30/B2, 40 wt % PB 64−60/B2, 20 wt % PB 64−80/B2, and 40 wt % PB 64−80/B2 blends, respectively. (These temperatures were chosen in a way that both of the fast and slow relaxation processes due to the arm relaxation and structural rearrangement were observed in our experimental window.) The shear stress $\sigma(t,\gamma)$ measured as a function of time t was summarized as the nonlinear relaxation modulus $G(t,\gamma) = \sigma(t,\gamma)/\gamma$.

Linear viscoelastic (dynamic) measurements were conducted at several temperatures including the T_r of respective blends. The amplitude of the oscillatory strain was kept small (≤0.05) to ensure the linearity of the storage and loss moduli $G'(\omega)$ and $G''(\omega)$ measured as functions of the angular frequency ω. The time−temperature superposition held for these G' and G'' data, and the data were reduced at T_r of respective blends.

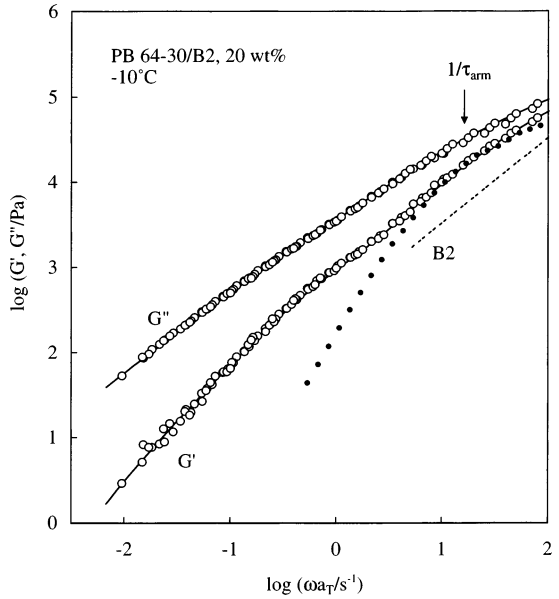

Figure 1. Linear viscoelastic behavior of 20 wt % PB 64−30 multiarm star/B2 blend at −10 °C (unfilled circles). The dotted curve indicates G'' of the pure matrix B2, and the small filled circles show G' of a solution of low-f star PB having the arm molecular weight and concentration identical to those of the multiarm star. The arrow indicates the relaxation frequency of individual multiarms. For further details, see text.

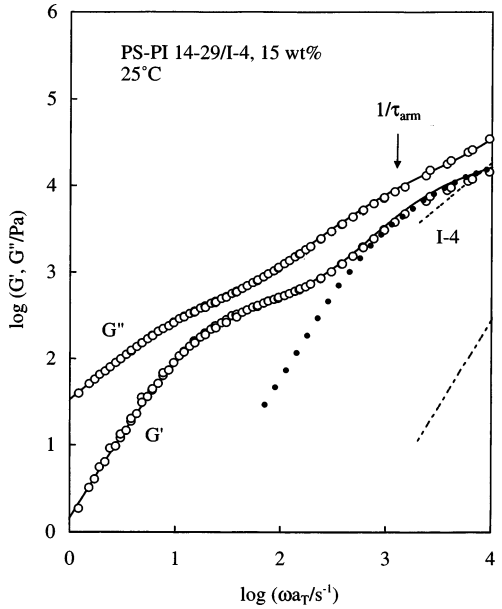

Figure 2. Linear viscoelastic behavior of 15 wt % PS−PI 14−29/I-4 micellar blend at 25 °C (unfilled circles; $10^{-3}M_S - 10^{-3}M_I$ = 13.9 − 28.8 for PS−PI 14−29 and $10^{-3}M$ = 4.1 for I-4).[9] The dotted curves indicate G' and G'' of the pure matrix I-4, and the small filled circles show G' of a solution of low-f star PI having the arm molecular weight and concentration identical to those of micellar corona PI blocks. The arrow indicates the relaxation frequency of individual corona blocks. For further details, see text.

For completeness of rheological characterization, stress−growth experiments after start-up of flow at various shear rates $\dot{\gamma}$ were conducted at T_r of respective blends, and the measured $\sigma(t,\dot{\gamma})$ was summarized as the viscosity growth function $\eta^+(t,\dot{\gamma}) = \sigma(t,\dot{\gamma})/\dot{\gamma}$. The steady-state viscosity was given by $\eta(\dot{\gamma}) = \eta^+(\infty,\dot{\gamma})$.

Before and after the measurements, GPC measurements were conducted to confirm no detectable oxidative cross-linking/degradation of the samples examined.

3. Results and Discussion

3.1. Linear Viscoelastic Behavior. Figure 1 shows angular frequency (ω) dependence of the storage and loss moduli G' and G'' of the 20 wt % PB 64−30/B2 blend at −10 °C (unfilled circles). The dotted line shows G'' of the matrix B2 at −10 °C. For comparison, Figure 2 shows the G' and G'' data obtained previously for a 15 wt % micellar dispersion (blend) of a PS−PI 14−29 diblock copolymer in a low-M homopolyisoprene (hI):[9] The molecular weights of the PS and PI blocks of this copolymer were $M_S = 13.9 \times 10^3$ and $M_I = 28.8 \times 10^3$, respectively, and the matrix (I-4) had $M = 4.1 \times 10^3$. (This M_I is close to M_{arm} of the PB 64−30 star arm, indicating that the unperturbed dimension is nearly the same for the PI block and PB star arm compared here.[28])

The PB 64−30 multiarm star has a soft, deformable core (of a Daoud−Cotton[29] radius ≅ 2 nm),[5] while the PS−PI micelle has a rigid, glassy S core (of the bare radius ≅ 8 nm.[9]). Despite this difference in the core softness, these materials exhibit qualitatively similar two-step relaxation processes, as seen in Figures 1 and 2. (The short matrices, B2 and I-4, have relaxed in the range of ω examined and do not contribute to this relaxation process.) A similar two-step relaxation was observed for all multiarm star PB/B2 blends examined as well as for bulk multiarm stars,[1,2,4,5] PS−PI/hI micellar blends having glassy PS cores,[8,9,18] and PB−PS/low-M homopolystyrene (hS) micellar blends having rubbery PB cores.[19]

The slow process of the multiarm star is attributed to the structural rearrangement (random exchange of the positions of neighboring stars) in the liquidlike order,[2−6] and the slow process of the copolymer micelle reflects the diffusion of the micelle (over a distance ≅ core diameter).[15−19] The fast processes of the multiarm star and copolymer micelle are commonly assigned to the orientational relaxation of individual star arms/corona blocks.[2−6,8,9,18,19] Indeed, we can confirm this assignment for the fast process by comparing the linear viscoelastic behavior of the multiarm star/copolymer micelle with the behavior of usual (low-f) stars with the arm number $f < 24$, as described below.

For the low-f star solutions, reduced moduli at low ω, G^*/C with C being the star concentration, are determined by a normalized frequency $\omega\tau_{star}$ (τ_{star} = relaxation time of the stars),[30] and the steady-state recoverable compliance is proportional to M_{arm},[31] meaning that the normalized linear viscoelastic moduli of the solutions of various C and M_{arm}, $M_{arm}G^*/C$, is universally dependent on $\omega\tau_{star}$ in the terminal regime. Considering this universality, we utilized G^* data of low-f homopolybutadiene (hB) and homopolyisoprene (hI) stars in the literature[30,32] to estimate G_{sol}^* of the low-f star solutions having M_{arm} and C identical to those of the multiarm star PB chains and the micellar corona PI blocks. In Figures 1 and 2, the G_{sol}' thus obtained are plotted against a shifted frequency $\omega\lambda$ (small filled circles). With appropriate choices of the values of the shift factor λ, these G_{sol}' agree well with the G' data of the multiarm star PB chains and the PS−PI micelles at high ω, confirming the previous finding[3,18,19] that the relaxation mode distribution of the fast process of the multiarm stars and micelles coincides with that of low-f stars and this process reflects the relaxation of individual multiarms/corona blocks. In addition, the agreement allows us to evaluate the arm/corona relaxation

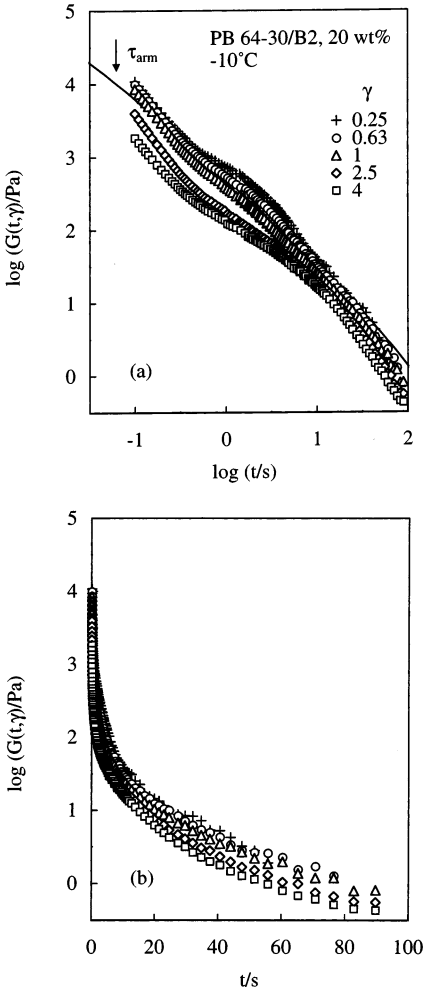

Figure 3. Nonlinear relaxation modulus $G(t,\gamma)$ of 20 wt % PB 64−30 multiarm star/B2 blend at −10 °C (symbols). Parts a and b respectively show the double-logarithmic and semilogarithmic plots of $G(t,\gamma)$ against t. The solid curve in (a) indicates the linear relaxation modulus $G(t)$ evaluated from the G' and G'' data shown in Figure 1.

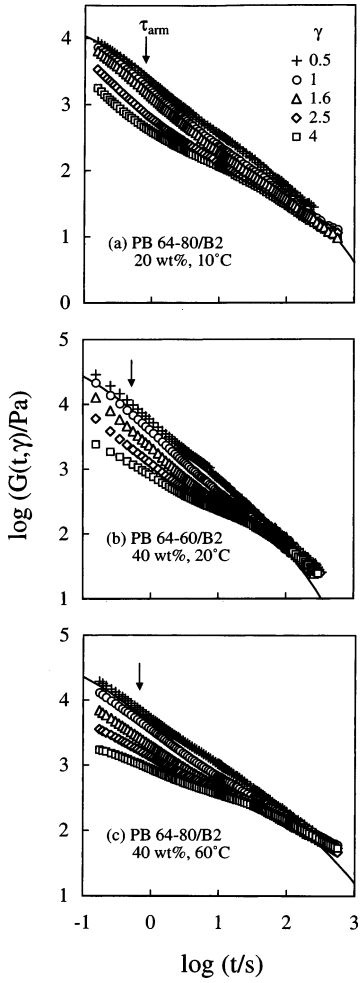

Figure 4. Nonlinear relaxation moduli $G(t,\gamma)$ of (a) 20 wt % PB 64−80/B2 blend at 10 °C, (b) 40 wt % PB 64−60/B2 blend at 20 °C, and (c) 40 wt % PB 64−80/B2 blend at 60 °C. The solid curves indicate the linear relaxation modulus $G(t)$.

time τ_{arm} in our blends from the known values of λ and the relaxation time of the low-f stars τ_{star} as $\tau_{arm} = \tau_{star}/\lambda$. This τ_{arm} well specifies the terminal frequency of the fast process; see the arrows in Figures 1 and 2.

Thus, the multiarm stars and copolymer micelles exhibit qualitative similarities in the linear viscoelastic regime. However, quantitative differences are also known. For example, the relaxation time of the fast process (= τ_{arm}) of the micelles is affected by the steric hindrance from the rigid and large S cores[8,9] while this effect is negligible for the multiarm stars having the soft and fairly small cores.[6]

Nonlinear rheological experiments revealed more striking differences between the multiarm stars and copolymer micelles. In the remaining part of this paper, these differences are discussed in relation to nonlinear features of related materials, concentrated homopolymer solutions,[33−35] Brownian suspensions of silica particles,[22,23] and a critical gel of poly(vinyl chloride).[36]

3.2. Nonlinear Relaxation Behavior. Figure 3 shows the nonlinear relaxation modulus $G(t,\gamma)$ of the 20 wt % PB 64−30/B2 blend at −10 °C. In parts a and b, the $G(t,\gamma)$ data are double-logarithmically and semilogarithmically plotted against the time t, respectively. In part a, the arrow and solid curve indicate the τ_{arm} of the arms and the relaxation modulus $G(t)$, both obtained in the linear viscoelastic regime. ($G(t)$ was evaluated from the G' and G'' data (Figure 1) with a previously reported iteration method.[37])

Fast and slow relaxation processes due to the arm relaxation and the structural rearrangement are clearly observed in Figure 3. (The matrix relaxation was too fast to be detected in our experimental window.) Both processes exhibit nonlinear decreases of the moduli with increasing strain γ up to 4, and this damping is much weaker for the slow process. This was the case for all multiarm star PB blends examined, as demonstrated in Figure 4. Similarly weak damping of the slow process was observed for polystyrene (PS) microgels having fairly short arms grafted thereon,[38,39] although the relaxation intensity of this process was considerably smaller for these microgels (having $f = 16-37$ arms per core of the microgel) than for the star PB chains examined in this study ($f = 56-61$).

For comparison with the nonlinear behavior of the multiarm stars, Figure 5 shows the $G(t,\gamma)$ data previously obtained for the 15 wt % PS−PI 14−29/I-4 micellar blend at 25 °C.[24] (The data were measured at −25, 5, and 25 °C, and the data at −25 and 5 °C were reduced at 25 °C.) Clearly, the nonlinear damping is much stronger for the slow process (micelle diffusion) than for the fast process (corona relaxation), as noted for all PS−PI micelles having rigid PS cores[8,18,24] and PB−PS micelles having soft PB cores.[19] Thus, the

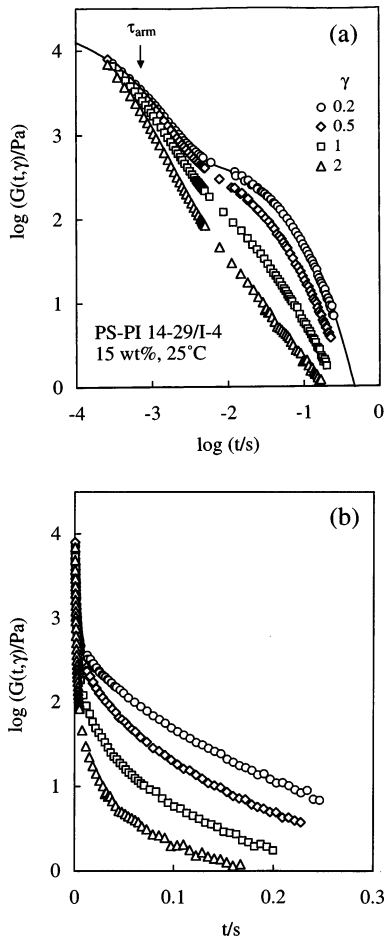

Figure 5. Nonlinear relaxation modulus $G(t,\gamma)$ of 15 wt % PS−PI 14−29/I-4 micellar blend reduced at 25 °C ($10^{-3}M_S - 10^{-3}M_I = 13.9 - 28.8$ for PS−PI 14−29 and $10^{-3}M = 4.1$ for I-4).[24] Parts a and b respectively show the double-logarithmic and semilogarithmic plots of $G(t,\gamma)$ against t. The solid curve in (a) indicates the linear relaxation modulus $G(t)$.

multiarm stars and copolymer micelles exhibit a striking difference in their nonlinear behavior at long t. This difference is later discussed in relation to the core softness and the core−arm interaction (compatibility).

At $t \gg \tau_{arm}$, the multiarms and the corona blocks have fully relaxed, and the $G(t,\gamma)$ data coincide with the nonlinear modulus for the slow process, $G_s(t,\gamma)$. For the multiarm stars and copolymer micelles examined in Figures 3−5, $G(t,\gamma)$ at such long t exhibits the damping, but its t dependence hardly changes with the strain, as most clearly noted for the semilogarithmic plots shown in Figures 3b and 5b. This fact indicates that $G_s(t,\gamma)$ of the multiarm stars and micelles obey the time−strain separability at long t, $G_s(t,\gamma) = G_s(t)h_s(\gamma)$ with $G_s(t)$ and $h_s(\gamma)$ being the linear relaxation modulus and the nonlinear damping function of the slow process, respectively.

The time−strain separability is valid for the slow process of the PS−PI and PB−PS copolymer micelles irrespective of the corona−corona and corona−matrix entanglements.[18,19,24] This is the case also for all multiarm star blends examined. (The arms are barely entangled in the blend examined in Figure 3 while they are mutually entangled in the blends examined in Figure 4.) The $h_s(\gamma)$ data of the multiarm stars and micelles are later compared with $h(\gamma)$ data of Brownian suspensions and a critical gel to discuss the damping mechanisms of the slow process.

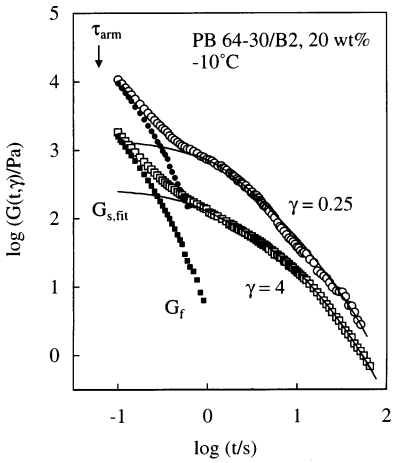

Figure 6. Separation of nonlinear relaxation modulus $G(t,\gamma)$ of 20 wt % PB 64−30 multiarm star/B2 blend for $\gamma = 0.25$ and 4 at −10 °C (unfilled symbols) into the moduli for the slow and fast processes (solid curves and small filled symbols).

3.3. Damping Functions. For the PS−PI micelles obeying the time−strain separability, we previously evaluated the damping function $h_s(\gamma)$ for the slow process as a vertical shift factor required for superposing the long-time tails of their $G(t,\gamma)$ data.[18,19,24] For evaluation of the relaxation modulus for the fast process, $G_f(t,\gamma)$, we focused on the $G(t,\gamma)$ data at sufficiently long t where this process had completed and the $G(t,\gamma)$ data coincided with $G_s(t,\gamma)$ for the slow process. Fitting these $G_s(t,\gamma)$ data with a sum of exponentially decaying function and subtracting this fitting function $G_{s,fit}(t,\gamma)$ from the $G(t,\gamma)$ data at short t, we obtained $G_f(t,\gamma)$ for the fast process.[18,19,24]

For the multiarm star chains examined in this study, we have applied the same method to evaluate $G_f(t,\gamma)$. Figure 6 shows a typical result of this evaluation for the 20 wt % PB 64−30 multiarm stars under the strains $\gamma = 0.25$ and 4: At $t > 20\tau_{arm}$ where the arms should have fully relaxed (cf. $\exp(-t/\tau_{arm}) \leq 2 \times 10^{-9}$ at $t > 20\tau_{arm}$), the $G(t,\gamma)$ data (unfilled symbols) were fitted with $G_{s,fit}$ ($= \sum_p g_p \exp(-t/\tau_p)$; solid curve), and this $G_{s,fit}$ was subtracted from the data to obtain $G_f(t,\gamma)$ (filled symbols). The $G_f(t,\gamma)$ determined in this way hardly changed even if the fitting was made in a wider range of t, $t > 10\tau_{arm}$ (where $\exp(-t/\tau_{arm}) \leq 5 \times 10^{-5}$), confirming a satisfactory accuracy of the $G_f(t,\gamma)$ data.

For the PS−PI and PB−PS micelles (having the PS and PB cores, respectively), the $G_f(t,\gamma)$ data obtained in this way satisfied the time−strain separability in the terminal regime of the fast process, $G_f(t,\gamma) = G_f(t)h_f(\gamma)$ with $G_f(t)$ and $h_f(\gamma)$ being the linear relaxation modulus and the damping function of this process.[18,19,24] For the multiarm stars, this separability is tested in Figure 7 where the $G_f(t,\gamma)$ data for various γ values are reduced by appropriately chosen h_f factors and plotted against t. The linear viscoelastic G^* data of these multiarm stars at intermediate ω were close to G_{sol}^* of solutions of low-functionality star PB chains having M_{arm} and C identical to those of multiarm stars, as demonstrated in Figure 1. In Figure 7, the linear relaxation moduli of those low-f star solutions $G_{sol}(t)$, evaluated from the G_{sol}^* data, are shown with the solid curves. The $h_f^{-1}G_f$ data of the multiarm stars exhibit good superposition at long t and are close to $G_{sol}(t)$, demonstrating the validity of the time−strain separability for the fast process of these stars.

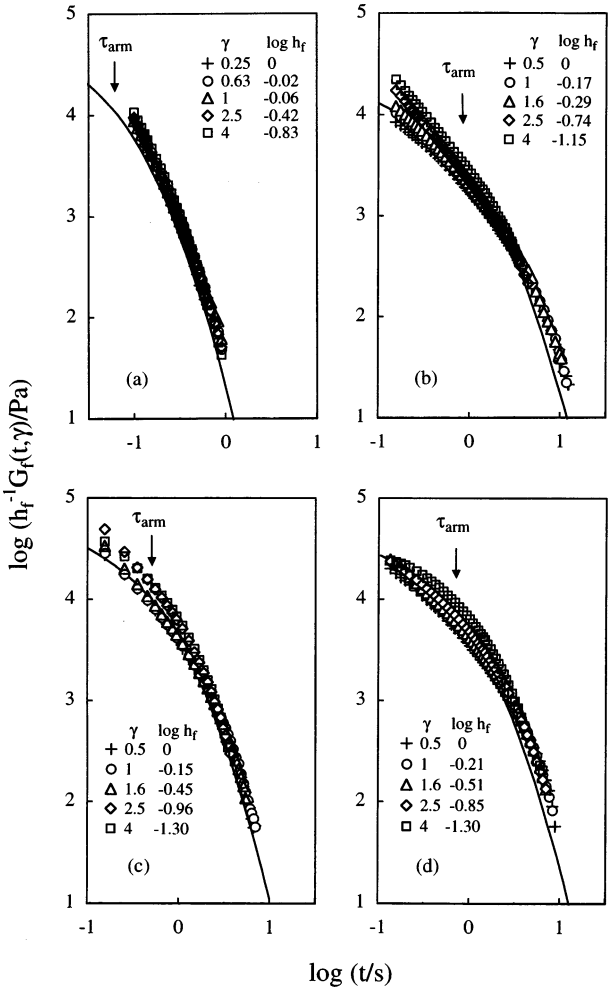

Figure 7. Comparison of the normalized moduli for the fast process, $h_f^{-1}G_f(t,\gamma)$, obtained for the multiarm star PB/B2 blends: (a) 20 wt % PB 64−30/B2 at −10 °C, (b) 20 wt % PB 64−80/B2 at 10 °C, (c) 40 wt % PB 64−60/B2 at 20 °C, and (d) 40 wt % PB 64−80/B2 at 60 °C.

Thus, the nonlinear features of the multiarm PB stars and the copolymer micelles are qualitatively similar in a sense that the time−strain separability holds for both of the fast and slow processes. However, the multiarm stars and micelles exhibit different magnitudes of damping, as noted for their $h_f(\gamma)$ and $h_s(\gamma)$ data summarized in Figures 8 and 9. As seen in Figure 8, the damping of the fast process is moderately stronger (h_f is smaller) for the multiarm stars (large unfilled symbols) than for the PS−PI and PB−PS micelles (large filled and half-filled symbols). This moderate difference can be noted also for the raw $G(t,\gamma)$ data at $t \sim \tau_{arm}$ (cf. Figures 3−5). In contrast, the damping of the slow process is much weaker (h_s is much larger) for the multiarm stars (see Figure 9). The h_s data of the previously examined low-M_{arm} PS microgel melts,[38] not shown in Figure 9 in order to avoid heavy overlapping of the plots, are close to the h_s data of the PB multiarm stars. The differences of the h data for the multiarm PB stars and PS−PI micelles are later discussed in relation to the damping behavior of the related materials, homopolymer solutions, Brownian suspensions of silica particles, and a critical gel of poly(vinyl chloride).

3.4. Non-Newtonian Flow Behavior. Figure 10a shows the viscosity growth function $\eta^+(t,\dot\gamma)$ of the 20 wt % PB 64−30/B2 blend at −10 °C. The dotted curve

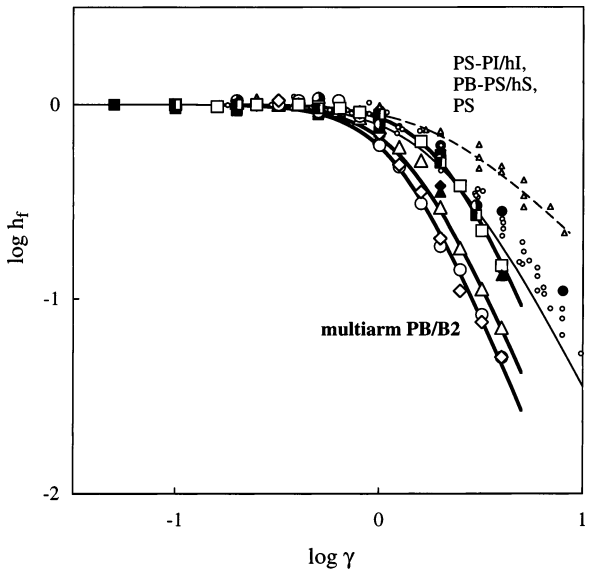

Figure 8. Damping function $h_f(\gamma)$ for the fast process of multiarm star PB chains in B2 (large unfilled symbols): square, PB 64−30 (20 wt %); diamond, PB 64−60 (40 wt %); triangle, PB 64−80 (20 wt %); circle, PB 64−80 (40 wt %). For comparison, $h_f(\gamma)$ data for the fast process of mutually entangled PS−PI micelles having PS cores are shown with the filled triangle (15 wt % PS−PI 68−122/I-2)[18] and filled diamond (15 wt % PS−PI 68−122/I-19).[18] The data for mutually nonentangled PS−PI and PB−PS micelles having PS and PB cores are shown with the filled square (15 wt % PS−PI 14−29/I-4),[24] filled circle (5 wt % PS−PI 68−122/I-19),[18] half-filled square (15 wt % PB−PS 16−81/S-11),[19] and half-filled circle (15 wt % PB−PS 26−63/S-11).[19] Here, the sample code numbers indicate $10^{-3}M$ of the blocks/homopolymer matrices, and the two PB−PS/S-11systems are plasticized with dibutyl phthalate (C_{DBP} = 24.1 wt %). Small unfilled circles and triangles show $h(\gamma)$ data[33−35] of entangled and nonentangled polystyrene solutions, respectively. The thin solid curve indicates the Doi−Edwards prediction without independent alignment approximation.

indicates the viscosity growth function in the linear regime, $\eta_L^+(t)$, evaluated from the linear $G(t)$ (solid curve in Figure 3a): $\eta_L^+(t) = \int_0^t G(t')\,dt'$. The $\eta^+(t,\dot\gamma)$ data decrease from this $\eta_L^+(t)$ with increasing shear rate $\dot\gamma$. Correspondingly, the steady-state viscosity $\eta(\dot\gamma)$ (= $\eta^+(\infty,\dot\gamma)$) decreases with $\dot\gamma$ (cf. Figure 10b). This thinning behavior was noted for all multiarm PB/B2 blends examined.

For the randomly dispersed PS−PI and PB−PS copolymer micelles (having rigid PS and soft PB cores, respectively), $\eta(\dot\gamma)$ exhibited two-step thinning with the decreases of $\eta(\dot\gamma)$ at low and high $\dot\gamma$ being governed by the nonlinearities of the slow and fast processes, respectively.[18,19,40] In contrast, the $\eta(\dot\gamma)$ data of the multiarm star PB decrease just gradually over a wide range of $\dot\gamma$ without exhibiting this two-step feature (see Figure 10b). We utilized the previous method (use of a constitutive equation)[18,19,40] to examine an origin of this gradual thinning. The results are summarized below.

If the non-Newtonian feature of the multiarm star reflects its nonlinear damping behavior under large strains, the $\eta^+(t,\dot\gamma)$ and $\eta(\dot\gamma)$ data should be described by a constitutive equation incorporating the damping data. Since the fast and slow relaxation processes of the multiarm star are time−strain separable, we may utilize a factorable BKZ constitutive equation incorporating the damping functions $h_f(\gamma)$ and $h_s(\gamma)$ and linear relaxation moduli $G_f(t)$ and $G_s(t)$ of respective processes.

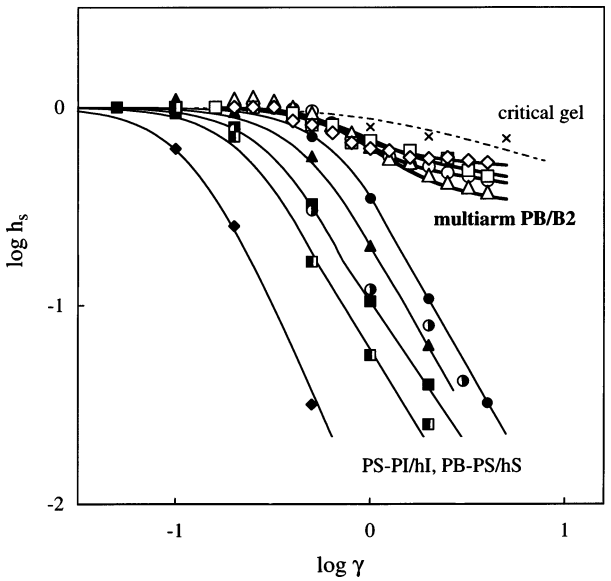

Figure 9. Damping function $h_s(\gamma)$ for the slow process of multiarm star PB chains in B2 (large unfilled symbols): square, PB 64−30 (20 wt %); diamond, PB 64−60 (40 wt %); triangle, PB 64−80 (20 wt %); circle, PB 64−80 (40 wt %). For comparison, $h_s(\gamma)$ data for the slow process of mutually nonentangled PS−PI micelles having PS cores are shown with large filled symbols (square, 15 wt % PS−PI 14−29/I-4;[24] circle, 15 wt % PS−PI 14−29/I-19;[18] triangle, 6 wt % PS−PI 43−86/I-4;[24] diamond, 12.8 wt % PS−PI 43−86/I-4[24]). The data for the mutually nonentangled PB−PS micelles having PB cores are shown with half-filled square (15 wt % PB−PS 16−81/S-11)[19] and half-filled circle (15 wt % PB−PS 26−63/S-11),[19] both systems being plasticized with dibutyl phthalate (C_{DBP} = 24.1 wt %). Here, the sample code numbers indicate $10^{-3}M$ of the blocks/homopolymer matrices. The cross symbol shows $h(\gamma)$ data of a critical gel of poly(vinyl chloride) in dioctyl phthalate ($M = 39.4 \times 10^3$, $C = 66$ g L^{-1}, $T = 49$ °C).[36]

Then, the viscosity growth function is calculated as[18,19,40,41]

$$\eta^+(t,\dot\gamma) = \phi_{mat}\eta_{mat} + \eta_f^+(t,\dot\gamma) + \eta_s^+(t,\dot\gamma) \qquad (1)$$

with

$$\eta_x^+(t,\dot\gamma) = G_x(t)h_x(\gamma_t)t - \int_0^t \frac{dG_x(t')}{dt'} h_x(\gamma_{t'})t'\,dt' \;(x = f, s) \qquad (2)$$

Here, ϕ_{mat} and η_{mat} are the volume fraction of the matrix B2 in the blend and the viscosity of the pure matrix, respectively, and γ_t (= $\dot\gamma \times t$) represents a strain in an interval of time from 0 to t imposed through the flow at the rate $\dot\gamma$.

In Figures 10a and 10b, the $\eta^+(t,\dot\gamma)$ and $\eta(\dot\gamma)$ (= $\eta^+(\infty,\dot\gamma)$) calculated from eqs 1 and 2 utilizing the $h_x(\gamma)$ and $G_x(t)$ data (x = f and s; cf. Figures 3a, 8, and 9) are shown with the solid curves. The dashed and dotted curves in Figure 10b show η_f (= $\eta_f^+(\infty,\dot\gamma)$) and η_s (= $\eta_s^+(\infty,\dot\gamma)$) calculated from eq 2. (Smooth fitting functions for $h_x(\gamma)$, shown with thick solid curves in Figures 8 and 9, were utilized in the calculation.) These calculated viscosities are satisfactorily close to the $\eta^+(t,\dot\gamma)$ and $\eta(\dot\gamma)$ data of the PB 64−30 multiarm star, suggesting that the thinning of this star reflects the nonlinear damping behavior under large strains. (Note that the weak damping of the slow process is still sufficient to give the observed non-Newtonian feature.) Similar results were obtained for all multiarm stars examined. Thus, the lack

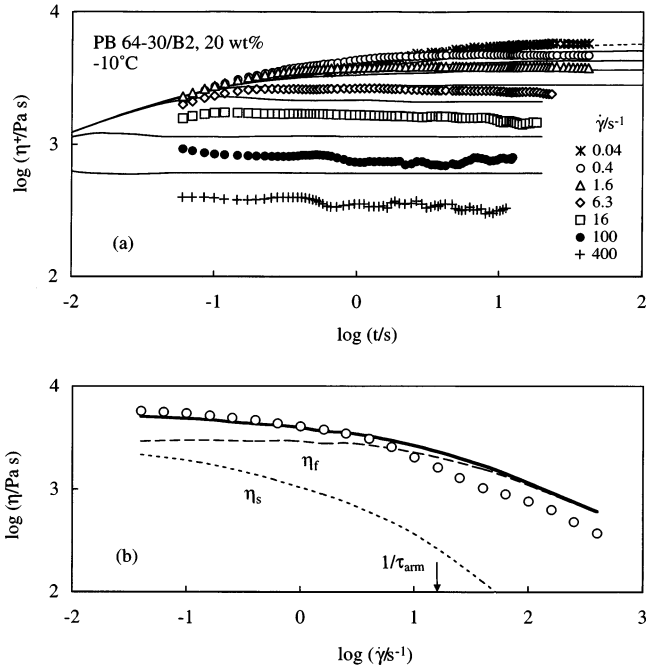

Figure 10. Viscosity growth function (a) and steady-state viscosity (b) of 20 wt % PB 64−30 multiarm star/B2 blend at −10 °C. In (a), the dotted curve indicates the growth function in the linear regime, and the solid curves show the nonlinear growth function calculated from a BKZ constitutive equation. In (b), the solid curves shows the steady-state viscosity calculated from the BKZ equation, and the dashed and dotted curves indicate the viscosities calculated for the fast and slow processes, respectively.

of the two-step thinning for the multiarm stars is attributed to the weak damping for the slow process that allows η_s to decrease just gradually and remain considerably large even at $\dot\gamma \cong 1/\tau_{arm}$ where η_f of the fast process begins to decrease (see Figure 10b). Correspondingly, the two-step thinning of the copolymer micelles[18,19,40] reflects the very strong damping for their slow process that leads to a significant decrease of $\eta_s(\dot\gamma)$ at $\dot\gamma \ll 1/\tau_{arm}$ where the fast process exhibits its zero-shear viscosity, $\eta_f(0)$.

3.5. Damping Mechanism of Slow Process. As demonstrated in Figure 9, the γ dependence of $h_s(\gamma)$ of the slow process is much weaker for the multiarm PB stars (unfilled symbols) than for the PS−PI and PB−PS micelles (filled and half-filled symbols). In addition to this quantitative difference, even a qualitative difference is noted: For the micelles, the damping is enhanced (i.e., $h_s(\gamma)$ decreases) as the concentration C increases while keeping the corona blocks in the nonentangled state; compare the large filled triangle and diamond for the 6 and 12.8 wt % blends of PS−PI 43−86 ($M_S = 43.2 \times 10^3$, $M_I = 85.8 \times 10^3$) in the I-4 matrix ($M_{I-4} = 4.1 \times 10^3$). The damping for the micelles is also enhanced when the corona−matrix entanglement vanishes; compare the large filled square and circle for the 15 wt % blends of PS−PI 14−29 ($M_S = 13.9 \times 10^3$, $M_I = 28.8 \times 10^3$) in the nonentangling I-4 and entangling I-19 matrices ($M_{I-19} = 19.0 \times 10^3$). In contrast, the $h_s(\gamma)$ data of the multiarm stars do not change significantly with C and M_{arm}. These differences should reflect an essential difference of the damping mechanisms of the multiarm stars and micelles, as discussed below.

Random suspensions of silica nanoparticles exhibit the time−strain separable, slow relaxation process governed by the particle diffusion, and the damping

function $h(\gamma)$ for this process strongly decreases with increasing particle content ϕ.[22,23] The viscoelastic stress of these particles, referred to as the Brownian stress σ_B, reflects an anisotropy in their spatial distribution raised by the applied strain γ.[42,43] For large γ, this anisotropy becomes insensitive to γ and thus σ_B does not increase in proportion to γ, which results in the nonlinear damping of $G(t,\gamma) = \sigma_B/\gamma$.[22,23] Concentrated particles collide with each other under large strains to exhibit nonaffine relative rotation, and this rotation is similar to random-mixing motion and reduces the anisotropy.[18,23] This collision-induced rotation occurs more significantly at larger ϕ to enhance the damping.

The $h_s(\gamma)$ data for the slow process of the PS−PI and PB−PS micelles are similar, in both magnitude and γ dependence, to $h(\gamma)$ data of the silica particles, as demonstrated in the previous papers.[8,18,19,40] This fact indicates that the damping mechanism is similar for the micelles and silica particles and the enhancement of the damping for concentrated micelles (Figure 9) is attributable to the relative rotational motion of these micelles activated by the applied strain. Furthermore, the weakening of the damping in the entangling matrix can be related to the matrix elasticity: The nonaffine relative rotation of the micelles, raising an extra strain in the matrix, would be suppressed in the elastic, entangling matrix compared to that in the less elastic, nonentangling matrix, thereby weakening the damping in the former matrix.[18]

Now, we turn our attention to the behavior of the multiarm stars. Since the stress of these stars in long time scales is related to a strain-induced distortion of their liquidlike order,[2,4] the damping for their slow process should reflect weakening of γ dependence of the magnitude of this distortion. For a focused star chain, the nearest-neighbor chains just before the application of strain (at $t = 0$) are displaced away by the large strain. However, the strain brings the other chains to the nearest-neighbor sites for the focused chain, and the number of these sites in the strain-distorted liquidlike order at $t > 0$ would become insensitive to γ for large γ, as similar to the situation for the silica particles/copolymer micelles. Thus, the magnitude of distortion of the liquidlike order of the multiarm stars would become insensitive to γ for large γ to raise the strong damping *if the focused chain does not distinguish its nearest neighbors before and after the application of strain*. However, the multiarm stars exhibit just weak damping of the slow process (Figure 9). This fact suggests that the chain makes this distinction, possibly due to a *strain-activated elastic coupling* between the chains neighboring at $t = 0$, as surmised for the polystyrene microgels having the grafted arms.[38,39] The coupled multiarm stars would behave as if they are fragments of a huge branched network, and the slow process (terminal relaxation) would be completed when these stars recover their initial arrangements to be released from the coupling. This situation is somewhat similar to that observed for pom-pom chains,[44,45] hyperbranched chains,[46−48] and a critical gel,[36] all having the inner part of the chain that can fully relax only after all outer parts relax: The damping of the inner part becomes weaker due to this constraint from the outer parts.[44,49] Indeed, a critical gel of poly(vinyl chloride) having the fractal network structure exhibits just weak damping, and its $h(\gamma)$ data[36] (cross symbols in Figure 9) are fairly close to the $h_s(\gamma)$ data of the multiarm stars (large unfilled symbols).

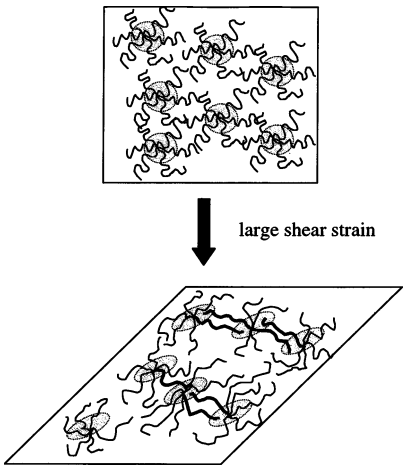

Figure 11. Schematic illustration of strain-induced elastic coupling of neighboring multiarm star chains. The soft core (gray circle) is considered to deform and become scarce under large strains to suck in segments of arms of neighboring chains, thereby forming a huge transient network that exhibits just weak damping.

With this molecular scenario, we now propose a mechanism(s) of the strain-induced elastic coupling at long t seen for the multiarm star chains. Since the strong damping is observed not only for the PS−PI micelles having rigid PS cores (filled symbols in Figure 9) but also for the PB−PS micelles with soft PB cores (half-filled symbols), this coupling mechanism should be unequivocally related to both of the core softness and the core−arm compatibility of the multiarm stars. Following the Daoud−Cotton picture,[29] we may consider the melt-like and solution-like regions in the core of a given multiarm star chain, the former being densely filled with the segments of this chain while the latter containing the segments of neighboring chains. The solution-like region is further divided into the inner, theta-like region and the outer, expanded region according to the conformation of the portions of the arms therein. The core containing these regions is in a soft, liquid state and should be significantly oriented and elongated on application of large step strains. Then, the strain may pull out a part of the segments of the given chain from the core, possibly from the theta-like region (and from the melt-like region as well), thereby making the core scarcer, which is somewhat similar to the situation for a network having the supercoiled conformation.[50,51] The elastic coupling/weak damping may occur for such elongated and scarce cores through the mechanism(s) discussed below.

The core would be subjected to a strong thermodynamic requirement of having the same segment density at equilibrium and under large strain. The elongated and scarce core of the given chain can preserve the equilibrium segment density therein without affecting the neighboring chains *if* it reduces its volume while keeping its orientation. However, this reduction in the volume would highly constrain the conformation of the portion of the given chain in the core, in particular in the theta-like region. Thus, the elongated and scarce core may suck in the arm segments of neighboring chains under large strains in order to loosen this constraint while keeping the equilibrium segment density therein, as schematically depicted in Figure 11: This sucking-in, probably occurring preferentially for

the segments near the arm ends to maximize the entropy of the sucked-in arms, is certainly possible because the core and arm are chemically identical and compatible. Then, the multiarm star chains under large strains are effectively bridged through these sucked-in arms (thick curves in Figure 11), thereby forming a huge branched network that preserves a memory of the initial arrangement of the chains coupled (bridged) on application of the large strain. The cores would be allowed to release the sucked-in segments and return to its equilibrium shape only when their initial arrangement is recovered, and the elastic energy stored in this network would relax only on this release. This slow relaxation should exhibit the weak damping because it has no significant route for dissipating the elastic energy in prior to its terminal stage. In relation to this point, we should note that full relaxation of the stress of the coupled arms incorporated in the network (thick curves in Figure 11) occurs during the slow process, not during the fast process assigned as the *independent relaxation of individual arms*.

With above mechanism, the elongated/scarce core would suck in the segments of surrounding chains without requiring a large-scale conformational change of these chains. Consequently, we expect that the sucking-in process is completed in a time scale considerably shorter than the time required for this conformational change, τ_{arm} (= arm relaxation time). A test of this expectation, achieved by observing the conformational changes in such short time scales with scattering methods (rather than by analyzing the $G_s(t,\gamma)$ data at short t obtained from the extrapolation of the $G(t,\gamma)$ data at long t; cf. Figure 6), is an interesting subject of future work.

The difference between the slow processes of the multiarm stars and the PS−PI/PB−PS micelles is attributable to the sucking-in mechanism that works for the stars having the soft cores chemically compatible with the arms but not for the micelles without this compatibility (and with undeformably rigid PS cores in the case of PS−PI micelles). In relation to this point, one may argue that the elastic energy stored in the deformed cores of the multiarm stars could weaken the damping at long t. However, *in the absence of the sucking-in mechanism*, the deformation of the cores should relax quickly (almost together with the arm relaxation that allows a rather large-scale motion of the core surface where the arm ends are connected). Then, the core deformation cannot contribute to the relaxation intensity of the slow process. This was indeed the case for the previously examined PS−PB micelles having the deformable PB cores[19] that similarly stored the elastic energy but exhibited the strong damping at long t (cf. half-filled symbols in Figure 9). Namely, the energy stored in the deformed cores may be released slowly to contribute to the weakening of the damping of the slow process of the multiarm stars, but this contribution emerges *only when* the stars are elastically coupled (through the sucking-in mechanism).

We should emphasize that the proposed sucking-in mechanism is still hypothetical, and a further study based on direct measurements of the core/arm structures under large strains is strongly desired. However, the difference between the micelles having either rigid or soft cores and the multiarm stars must be unequivocally related to the mechanical softness of the star cores and the chemical compatibility between these cores and the star arms.

3.6. Damping Mechanism of Fast Process. In Figure 8, small unfilled circles and triangles show the $h(\gamma)$ data of entangled[33,34] and nonentangled[35] polystyrene solutions, and the filled and half-filled symbols indicate representative $h_f(\gamma)$ data for the fast process of the PS−PI and PB−PS micelles (relaxation of individual corona blocks). The data for the micelles mutually entangled through their corona are shown with the filled triangle and diamond, and those for the mutually nonentangled micelles are denoted with the filled and half-filled square and circle. For the entangled chains, the thin solid curve indicates the prediction of the Doi−Edwards (DE) theory[31,52] without the independent alignment approximation.

The $h_f(\gamma)$ data for the micelles are close to the homopolymer data (and the DE prediction), demonstrating that the damping of this process is similar to that for the homopolymers and attributable to the retraction of the strain-elongated corona blocks occurring in prior to their rotational motion (orientational relaxation).[8,18,19,24,53] A detailed inspection indicates that the $h_f(\gamma)$ data of the mutually nonentangled and entangled corona blocks are close to but a little smaller than the $h(\gamma)$ data of nonentangled and entangled homopolymers. This small difference is partly attributable to the filler effect from the micellar PS cores (that increases a local strain in the corona phase to enhance the damping)[18] and to a coupling between the corona retraction and the PB core relaxation.[19] Despite this small difference, the nonlinear features of the corona blocks seen in the fast process are essentially the same as those of the homopolymers.

In principle, this similarity with the homopolymers should be found also for the fast process of the multiarm stars reflecting the independent relaxation of individual arms. However, the $h_f(\gamma)$ values for this process (large unfilled symbols in Figure 8) are certainly smaller than the $h(\gamma)$ values for the homopolymers. This difference can be related to the feature of the slow process of the multiarm stars. The weak damping of the slow process is attributable to the strain-induced elastic coupling of the neighboring stars occurring through the formation of the transient network, as discussed above. The arms incorporated in this network would release their elastic energy during the slow process, meaning that these arms do not contribute to the relaxation intensity of the fast process. Since more segments would be sucked into the deformed cores and thus more arms would be incorporated in the transient network under larger strain γ, the relaxation intensity of the fast process would decrease with γ more strongly compared to that for the homopolymers. The fairly strong damping observed for the fast process of the multiarm stars would reflect this situation.

Archer and Juliani[45] reported that the damping at the long-time end of the relaxation process is stronger for well-entangled 6-arm star PB than for linear and/or pom-pom PB of similar entanglement density. One may suspect that the moderately strong damping of the fast process of our multiarm star PB is similar to that of the 6-arm star PB. However, we should emphasize that the damping of the fast process is considerably stronger than that reported for the 6-arm star PB: For $\gamma = 4$ (the largest strain examined in this study), $h_f(\gamma) \cong 0.05$ for well-entangled multiarm stars (see the unfilled circle

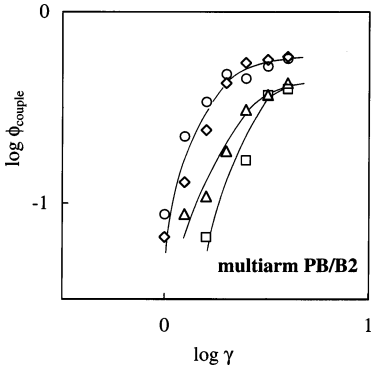

Figure 12. Dependence of fraction of elastically coupled arms, ϕ_{couple} (eq 3), on strain γ: square, PB 64−30 (20 wt %); diamond, PB 64−60 (40 wt %); triangle, PB 64−80 (20 wt %); circle, PB 64−80 (40 wt %).

and diamond in Figure 8) while $h(\gamma) \cong 0.09$ for the 6-arm star PB (see Figure 10 of ref 45). Thus, the moderately strong damping of the fast process of the multiarm stars should reflect a unique feature of these stars. This feature is discussed below in more detail.

3.7. Analysis of Interplay between Damping of Fast and Slow Processes. The molecular scenario explained for the slow and fast processes of the multiarm stars suggests that the magnitudes of damping of these processes are mutually correlated. With this scenario, a difference between the h_f data for the fast process of the micellar corona and star arm is mainly related to the number of the elastically coupled arms (the arms incorporated in the transient network through their sucked-in segments). Assuming that the magnitude of damping defined for each uncoupled arm is similar to that for a corona block, we may roughly estimate the fractions of the uncoupled and coupled arms from the h_f data (Figure 8) as

$$\phi_{uncouple}(\gamma) \cong \frac{h_f^{multiarm}(\gamma)}{h_f^{micelle}(\gamma)}, \quad \phi_{couple}(\gamma) = 1 - \phi_{uncouple}(\gamma) \tag{3}$$

We have utilized the $h_f^{micelle}$ data for the 15 wt % PS−PI 68−122/I-2 (filled triangle) and 5 wt % PS−PI 68−122/I-19 (filled circle) as the reference data for the entangled and nonentangled multiarm stars to estimate the ϕ_{couple} values of these stars. In Figure 12, this ϕ_{couple} is double-logarithmically plotted against the strain γ. The ϕ_{couple} value becomes well above zero and the sucking-in appears to occur significantly for strains larger than a critical strain γ_c; $\gamma_c \cong 1$ for the 40 wt % PB 64−80 and PB 64−60 systems and 20 wt % PB 64−80 system (circles, diamonds, and triangles), and $\gamma_c \cong 1.6$ for the 20 wt % PB 64−30 system (squares). We also note that ϕ_{couple} increases with increasing γ ($> \gamma_c$) and tends to level off at large γ. This leveling-off value, ϕ_{couple}^{∞}, is estimated to be ≅0.6 for the 40 wt % PB 64−80 and PB 64−60 systems and ≅0.4 for the 20 wt % PB 64−80 and PB 64−30 systems. These tendencies are in harmony with the molecular scenario of strain-induced sucking-in: For a given γ, the initial stress σ_0 due to the step strain increases as the system becomes more concentrated and entangled, and this increase of σ_0 would result in a larger deformation of the cores to enhance the sucking-in, thereby reducing γ_c and increasing ϕ_{couple}^{∞}.

In relation to the ϕ_{couple}^{∞} value, we note that the large step shear strain stretches the arm significantly if the end-to-end vector of this arm just before application of the strain, $\mathbf{R}_0$, is oriented in the shear-gradient direction while no stretching occurs for the arms having $\mathbf{R}_0$ in the shear and vorticity directions. Thus, on average, one-third of the arms are stretched by the strain and the two-thirds remain in the unstretched state. The pulling out of the segments from the core would occur for the stretched arms having a large tension, and the sucking-in of the segments (thermodynamically required compensation of the pulled out segments) would occur preferentially for the unstretched arms: The unstretched arms are in the entropically favorable state and can bear a conformational constraint due to this sucking-in. Then, under large strains, the sucking-in is expected to occur for two-thirds of the arms. (In addition, this sucking-in might occur preferentially in the shear-vorticity plane in which $\mathbf{R}_0$ of these arms is oriented before application of the strain, as schematically shown in Figure 11.) Interestingly, the ϕ_{couple}^{∞} values estimated above are close to this expectation, in particular for the mutually entangled arms ($\phi_{couple}^{\infty} \cong 0.6$). This result seems to lend support to our hypothesis of the sucking-in mechanism.

It is of interest to further examine a relationship between ϕ_{couple}^{∞} and the damping function for the slow process of the multiarm stars, $h_s^{star}(\gamma)$. The stress of the multiarm stars in long time scales would be given as a sum of the thermodynamic stress σ_{th} due only to the distortion of the liquidlike order of the star cores and the rubbery stress σ_r due to the elastically coupled arms in the transient network. Assuming that the damping of σ_{th} is similar to the damping of the Brownian stress σ_B of the micelles and described by $h_s^{micelle}(\gamma)$ of the micelles having the core concentration similar to that for the multiarm stars, we may express $h_s^{star}(\gamma)$ as

$$h_s^{star}(\gamma) = \frac{G_{s,fit}^{star}(0)\, h_s^{micelle}(\gamma) + G_e^{couple}}{G_{s,fit}^{star}(0)} \cong \frac{G_e^{couple}}{G_{s,fit}^{star}(0)} \quad \text{for large } \gamma \tag{4}$$

Here, $G_{s,fit}^{star}(0)$ is the initial modulus of the slow process of the multiarm stars in the linear viscoelastic regime (obtained from the fitting explained in Figure 6), and G_e^{couple} is the equilibrium modulus of the coupled arms that is to be observed when the cores do not release the sucked-in segments and the transient network does not relax. Since $h_s^{micelle}(\gamma)$ decreases significantly with increasing γ irrespective of the core concentration (cf. Figure 9), $h_s^{star}(\gamma)$ for large γ can be simply estimated as the $G_e^{couple}/G_{s,fit}^{star}(0)$ ratio, as indicated in eq 4.

The simplest estimate of the modulus of the coupled arms, being based on the concept of rubber elasticity, is given by $G_e^{couple} = \nu kT\phi_{couple}^{\infty}$, where ν, k, and T are the total number density of the arms (evaluated from the known concentration and molecular weight of the arm), Boltzmann constant, and absolute temperature, respectively, and ϕ_{couple}^{∞} is the fraction of the elastically coupled arms for large γ. However, we need to make corrections for this simple estimate. G_e^{couple} would be affected by the local osmotic interaction (that introduces correlation among the chains to effectively reduce ν)[10] and may also exhibit some weak nonlinearity under large strains (as observed for usual cross-linked rub-

Table 2. Comparison of Estimated and Measured h_s of the Multiarm Star PB Chains

system	estimated h_s[a]	measured h_s[b]
20 wt % PB 64−30/B2	0.70	0.45
40 wt % PB 64−60/B2	0.71	0.52
20 wt % PB 64−80/B2	0.53	0.37
40 wt % PB 64−80/B2	0.60	0.43

[a] $h_s = 0.1\nu kT\phi^{\infty}_{couple}/G^{star}_{s,fit}(0)$ estimated for large γ. [b] Data measured for the largest strain examined, $\gamma = 4$.

bers[54,55]). The correction for the local osmotic effect may be made on the basis of the experimental observation that the PS−PB micelles with PS cores and PB corona has the equilibrium modulus $G_e \cong 0.1\nu kT$ when they are arranged on a cubic lattice due to the osmotic effect.[10] The factor of ≅0.1 represents the reduction of ν due to this effect. In Table 2, the estimate of the damping function corrected for this factor, $h_s^{star} \cong 0.1\nu kT\phi^{\infty}_{couple}/G^{star}_{s,fit}(0)$, is compared with the $h_s(\gamma)$ data of the multiarm stars obtained for $\gamma = 4$ (largest γ examined). The estimated h_s is fairly close to the measured h_s and reproduces the tendency of changes of the measured h_s with M_{arm} and C_{arm}.

Since this estimate of h_s was obtained under the assumption of similarity between σ_{th} and σ_B and was not corrected for the expected nonlinearity of G_e^{couple}, the results seen in Table 2 are to be interpreted only qualitatively. At the same time, we should point out that these results are consistent with the molecular scenario of the strain-induced formation of the transient network through sucking-in of the segments.

4. Concluding Remarks

We have examined the nonlinear relaxation behavior of the multiarm PB star chains under large strains and compared the results with the behavior of random dispersions of PS−PI and PB−PS diblock copolymer micelles (having rigid PS and soft PB cores, respectively). All these materials exhibited the fast and slow relaxation processes attributed to the orientational relaxation of individual arms/corona blocks and motion of the cores. However, the nonlinear damping for the slow process was much weaker for the multiarm stars than for the PS−PI/PB−PS micelles, while the damping for the fast process was moderately stronger for the multiarm stars. A corresponding difference between the multiarm stars and micelles was noted for the viscosity under shear flow.

These differences should reflect the softness of the multiarm star cores and the compatibility of the chemically identical core and arms. Specifically, we note a possibility that the star core is deformed by the applied large strain and becomes scarcer when a part of the segments therein is pulled out by the strain. Then, the scarce core may suck in some segments of the neighboring multiarm stars to preserve its equilibrium segment density while keeping the constraint for the conformation of the portion of the arm therein to a low level. This leads to formation of a huge transient network of the arms elastically coupled through the sucked-in segments. These coupled arms should increase the terminal relaxation intensity of the slow process, thereby weakening the damping for this process and enhancing the damping for the fast process. No similar mechanism works for the PS−PI and PB−PS micelles having the cores chemically incompatible with the corona blocks. (In addition, for the PS−PI micelles, the PS cores are glassy so that the sucking-in mechanism is completely ruled out.)

The above molecular scenario, though still hypothetical, allows us to relate the differences of the nonlinear behavior of the multiarm stars and micelles to the core softness and arm−core compatibility. A test of this scenario though direct observation of the core/arm structure is considered as an important subject of future work.

References and Notes

(1) Vlassopoulos, D.; Pakula, T.; Fytas, G.; Roovers, J.; Karatasos, K.; Hadjichristidis, N. *Eur. Phys. Lett.* **1997**, *39*, 617.
(2) Pakula, T.; Vlassopoulos, D.; Fytas, G.; Roovers, J. *Macromolecules* **1998**, *31*, 8931.
(3) Vlassopoulos, D.; Fytas, G.; Fleischer, G.; Pakula, T.; Roovers, J. *Faraday Discuss.* **1999**, *112*, 225.
(4) Kapnistos, M.; Semenov, A. N.; Vlassopoulos, D.; Roovers, J. *J. Chem. Phys.* **1999**, *111*, 1753.
(5) Vlassopoulos, D.; Fytas, G.; Pakula, T.; Roovers, J. *J. Phys.: Condens. Matter* **2001**, *13*, R855.
(6) Miros, A.; Vlassopoulos, D.; Likhtman, A. E.; Roovers, J. *J. Rheol.* **2003**, *47*, 163.
(7) Watanabe, H.; Kotaka, T.; Hashimoto, T.; Shibayama, M.; Kawai, H. *J. Rheol.* **1982**, *26*, 153.
(8) Watanabe, H. *Acta Polym.* **1997**, *48*, 215.
(9) Sato, T.; Watanabe, H.; Osaki, K.; Yao, M. L. *Macromolecules* **1996**, *29*, 3881.
(10) Watanabe, H.; Kanaya, T.; Takahashi, Y. *Macromolecules* **2001**, *34*, 662.
(11) Watanabe, H.; Matsumiya, Y.; Kanaya, T.; Takahashi, Y. *Macromolecules* **2001**, *34*, 6742.
(12) Watanabe, H.; Kotaka, T. *J. Rheol.* **1983**, *27*, 223.
(13) Watanabe, H.; Sato, T.; Osaki, H. *Macromolecules* **1996**, *29*, 104.
(14) Watanabe, H.; Sato, T.; Osaki, H. *Macromolecules* **1996**, *29*, 113.
(15) Watanabe, H.; Sato, T.; Osaki, K.; Hamersky, M. W.; Chapman, B. R.; Lodge, T. P. *Macromolecules* **1998**, *31*, 3740.
(16) Gohr, K.; Pakula, T.; Tsutsumi, K.; Schartl, W. *Macromolecules* **1999**, *32*, 7156.
(17) Gohr, K.; Schartl, W. *Macromolecules* **2000**, *33*, 2129.
(18) Matsumiya, Y.; Watanabe, H. *Macromolecules* **2004**, *37*, 9861.
(19) Watanabe, H.; Matsumiya, Y. *Macromolecules* **2005**, *38*, 3808.
(20) Mellema, J.; van der Werff, J. C.; Blom, C.; de Kruif, C. G. *Phys. Rev. A* **1989**, *39*, 3696.
(21) Shikata, T.; Pearson, D. S. *J. Rheol.* **1994**, *38*, 601.
(22) Watanabe, H.; Yao, M. L.; Yamagishi, A.; Osaki, K.; Shikata, T.; Niwa, H.; Morishima, Y. *Rheol. Acta* **1996**, *35*, 433.
(23) Watanabe, H.; Yao, M. L.; Osaki, K.; Shikata, T.; Niwa, H.; Morishima, Y. *Rheol. Acta* **1999**, *38*, 2.
(24) Watanabe, H.; Sato, T.; Osaki, K.; Yao, M. L. *Macromolecules* **1996**, *29*, 3890.
(25) Roovers, J.; Zhou, L. L.; Toporowski, P. M.; van der Zwan, M.; Iatrou, H.; Hadjichristidis, N. *Macromolecules* **1993**, *26*, 4324.
(26) The lack of the entanglement in the 20 wt % PB 64−30/B2 system and the existence of the entanglement in the other three systems can be concluded even if we utilize the simplest dilution exponent, 1.0, to evaluate the reduced molecular weight as $M_{arm}\phi_{arm}$.
(27) Ferry, J. D. *Viscoelastic Properties of Polymers,* 3rd ed.; Wiley: New York, 1980.
(28) (a) For PI and PB chains having the same M, the unperturbed dimension agrees within 10%.[28b] (b) Kurata, M.; Tsunashima, Y. *Viscosity-Molecular Weight Relationships and Unperturbed Dimension of Linear Chain Molecules*. In *Polymer Handbook*, 3rd ed.; Brandrup, J., Immergut, E. H., Eds., Wiley: New York, 1989; Chapter VII.
(29) Daoud, M.; Cotton, J. P. *J. Phys. (Paris)* **1982**, *43*, 531.
(30) Raju, V. R.; Menezes, E. V.; Marin, G.; Graessley, W. W.; Fetters, L. J. *Macromolecules* **1981**, *14*, 1668.
(31) Watanabe, H. *Prog. Polym. Sci.* **1999**, *24*, 1253.
(32) Fetters, L. J.; Kiss, A. D.; Pearson, D. S.; Quack, G. F.; Vitus, F. J. *Macromolecules* **1993**, *26*, 647.
(33) Osaki, K.; Nishizawa, K.; Kurata, M. *Macromolecules* **1982**, *15*, 1068.
(34) Osaki, K.; Takatori, E.; Kurata, M.; Watanabe, H.; Yoshida, H.; Kotaka, T. *Macromolecules* **1990**, *23*, 4392.

(35) Takatori, E.; Osaki, K.; Kurata, M.; Hirayama, T. *Nihon Reoroji Gakkaishi (J. Soc. Rheol. Jpn.)* **1988**, *16*, 99.
(36) Watanabe, H.; Sato, T.; Osaki, K.; Aoki, Y.; Li, L.; Kakiuchi, M.; Yao, M. L. *Macromolecules* **1998**, *31*, 4198.
(37) Watanabe, H.; Matsumiya, Y.; Inoue, T. *Macromolecules* **2002**, *35*, 2339.
(38) Yamamoto, T.; Ohta, Y.; Takigawa, T.; Masuda, T. *Nihon Reoroji Gakkaishi (J. Soc. Rheol. Jpn.)* **2002**, *30*, 129.
(39) Yamamoto, T.; Ishimura, Y.; Takigawa, T.; Masuda, T. *Nihon Reoroji Gakkaishi (J. Soc. Rheol. Jpn.)* **2003**, *31*, 143.
(40) Watanabe, H.; Yao, M. L.; Sato, T.; Osaki, K. *Macromolecules* **1997**, *30*, 5905.
(41) The $\phi_{mat}\eta_{mat}$ term in eq 1 hardly contributed to the calculated $\eta^+(t,\dot{\gamma})$. Thus, in the calculation, we have neglected a possible change in η_{mat} of the short matrix B2 chains due to a small change in their monomeric friction on blending with much longer multiarm star PB chains.
(42) Brady, J. F. *J. Chem. Phys.* **1993**, *99*, 567.
(43) Bender, J. W.; Wagner, N. J. *J. Colloid Interface Sci.* **1995**, *172*, 171.
(44) Archer, L. A.; Varshney, S. K. *Macromolecules* **1998**, *31*, 6348.
(45) Archer, L. A.; Juliani *Macromolecules* **2004**, *37*, 1076.
(46) Garcia-Franco, C. A.; Srinivas, S.; Lohse, D.; Brant, P. *Macromolecules* **2001**, *34*, 3115.
(47) Wood-Adams, P. M.; Dealy, J. M. *Macromolecules* **2000**, *33*, 7481.
(48) Wood-Adams, P. M.; Dealy, J. M.; deGroot, A. W.; Redwine, O. D. *Macromolecules* **2000**, *33*, 7489.
(49) (a) For the hierarchical relaxation of hyper-branched chains (including the pom-pom chains), the damping strength in long time scales has been analyzed by Bick and McLeish.[49b] (b) Bick, D. K.; McLeish, T. C. B. *Phys. Rev. Lett.* **1996**, *76*, 2587.
(50) Urayama, K.; Kohjiya, S. *Eur. Phys. J. B* **1998**, *2*, 75.
(51) Obukov, S. P.; Rubinstein, M.; Colby, R. H. *Macromolecules* **1994**, *27*, 3191.
(52) Doi, M.; Edwards, S. F. *The Theory of Polymer Dynamics*, Clarendon: Oxford, 1986.
(53) It should be noted that the time−strain separable nonlinear damping occurs not only for entangled homopolymers[33,34] but also for nonentangled homopolymers,[35] although the damping is weaker for the latter. This fact means that the nonentangled chains under large strains exhibit retraction in prior to their rotational motion,[31] although details of this retraction mechanism have not been fully elucidated.
(54) Erman, B.; Mark, J. E. *Structure and Properties of Rubberlike Networks*; Oxford University Press: Oxford, 1997.
(55) Urayama, K.; Kawamura, T.; Kohjiya, S. *Macromolecules* **2001**, *34*, 8261.

MA0506738